New investigations at Kalambo Falls, Zambia

Duller, G. A. T.; Tooth, Stephen; Barham, Lawrence; Tsukamoto, Sumiko

New investigations at Kalambo Falls, Zambia: Luminescence chronology, site formation, and archaeological significance

Geoff A.T. Duller [a, *], Stephen Tooth [a], Lawrence Barham [b], Sumiko Tsukamoto [c]

[a] Department of Geography and Earth Sciences, Aberystwyth University, Aberystwyth, SY23 3DB, UK
[b] Department of Archaeology, Classics and Egyptology, University of Liverpool, L69 3GS, UK
[c] Leibniz Institute for Applied Geophysics, Geochronology and Isotope Hydrology, Stilleweg 2, Hannover D-30655, Germany

A B S T R A C T

Fluvial deposits can provide excellent archives of early hominin activity but may be complex to interpret, especially without extensive geochronology. The Stone Age site of Kalambo Falls, northern Zambia, has yielded a rich artefact record from dominantly fluvial deposits, but its significance has been restricted by uncertainties over site formation processes and a limited chronology. Our new investigations in the centre of the Kalambo Basin have used luminescence to provide a chronology and have provided key insights into the geomorphological and sedimentological processes involved in site formation. Excavations reveal a complex assemblage of channel and floodplain deposits. Single grain quartz optically stimulated luminescence (OSL) measurements provide the most accurate age estimates for the youngest sediments, but in older deposits the OSL signal from some grains is saturated. A different luminescence signal from quartz, thermally transferred OSL (TT-OSL), can date these older deposits. OSL and TT-OSL results are combined to provide a chronology for the site. Ages indicate four phases of punctuated deposition by the dominantly laterally migrating and vertically aggrading Kalambo River (~500–300 ka, ~300–50 ka, ~50–30 ka, ~1.5–0.49 ka), followed by deep incision and renewed lateral migration at a lower topographic level. A conceptual model for site formation provides the basis for improved interpretation of the generation, preservation, and visibility of the Kalambo archaeological record. This model highlights the important role of intrinsic meander dynamics in site formation and does not necessarily require complex interpretations that invoke periodic blocking of the Kalambo River, as has previously been suggested. The oldest luminescence ages place the Mode 2/3 transition between ~500 and 300 ka, consistent with other African and Asian sites where a similar transition can be found. The study approach adopted here can potentially be applied to other fluvial Stone Age sites throughout Africa and beyond.

1. Introduction

Kalambo Falls, located in northern Zambia on the Tanzanian border (Fig. 1a, b), was the site of detailed archaeological excavations between 1956 and 1966. Deposits in a basin upstream of the falls produced one of the most important artefact archives spanning the late Acheulean (Mode 2) to early Middle Stone Age (Mode 3) transition in south-central Africa (Clark, 1969, 2001). Owing to the rich record of artefacts recovered from the site and the limited number of other stratified sequences covering the Mode 2 to Mode 3 transition in this part of Africa, Kalambo Falls could potentially play an important role in discussions about the timing and importance of the characteristic technological changes of this transition (Barham et al., 2009). The significance of the Kalambo Falls record, however, has been diminished by uncertainties about the geomorphological and sedimentological processes involved in site generation and preservation (Sheppard and Kleindienst, 1996; Schick, 2001) and by a very limited chronology (Clark, 2001), thereby contributing to the marginalisation of the site in such discussions. All four of Clark's (1969, 2001) excavations (designated sites A, B, C, and D) are immediately adjacent to the Kalambo River, and while fluvial processes are known to have played a key role in site formation (e.g., Schick, 2001), many uncertainties surround the nature, timing, and controls of river and floodplain activity.

While it is recognised that fluvial deposits can provide excellent archives of early hominin activity (Mishra et al., 2007), most

* Corresponding author.
    E-mail address: ggd@aber.ac.uk (G.A.T. Duller).
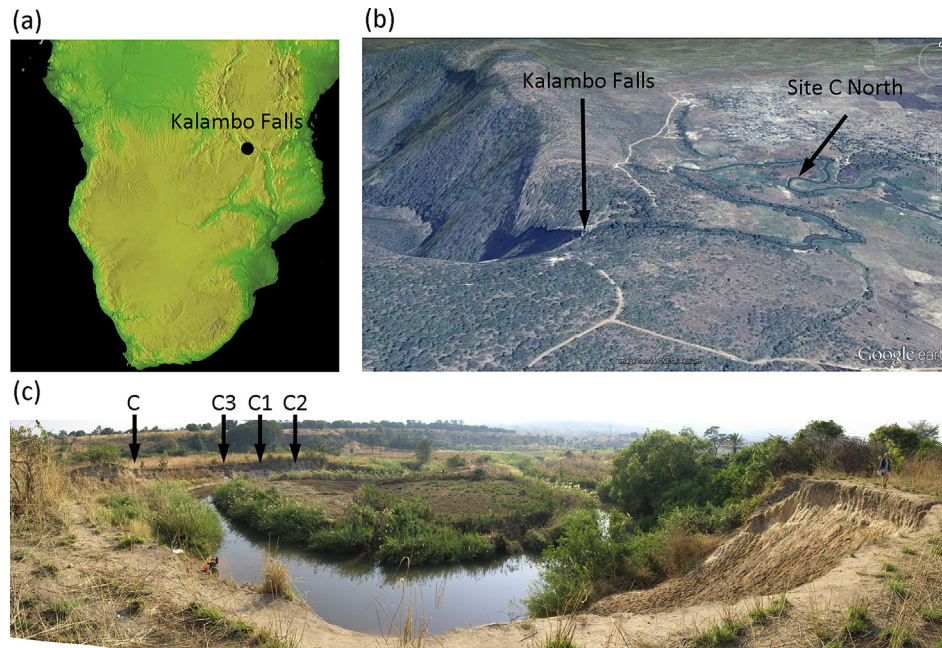
Figure 1. a) Digital Elevation Model of the southern part of the African continent (from NASA) showing the location of Kalambo Falls at the southern end of one arm of the East African Rift Systems (now partly occupied by Lake Tanganyika). b) Oblique aerial view of the Kalambo River meandering through the small Kalambo Basin (flow direction from right to left) prior to its ~200 m long passage through a quartzite ridge (spillway gorge) and over Kalambo Falls. Image taken from Google Earth. c) Panoramic view of Site C North. The Kalambo River flows from centre right to upper left and the meander bend shown in this photograph is indicated by an arrow in (b). Note how the modern channel is incised up to 9 m below the surface of the basin fill, with lateral migration and renewed floodplain formation now taking place at a lower topographic level. The original Site C of Clark (2001) is thought to have been located near to the foreground of this image but has been eroded by the ongoing meander bend migration. Excavations in 2006 took place at locations shown by arrows on the left of the image where recent erosion had provided near-vertical exposures.

attention has focused on flights of alluvial river terraces, as these represent former floodplains within which archaeological materials may be preserved and placed in a relative chronology (e.g., Bridgland, 2006; Gibbon et al., 2009). In the Kalambo Basin and some other important fluvial archaeological sites worldwide, however, rivers have not undergone the episodic net incision necessary to generate alluvial terrace flights. In these situations, basin or valley alluvial fills containing important archaeological material may be generated and preserved (e.g., Lewin and Macklin, 2003) but the sedimentary archives may be more complex to interpret than those characterising terrace flights, and without deep incision and/or extensive gully formation, the archaeological record may remain largely or completely invisible (e.g., Brink et al., 2012; Tooth et al., 2013).

In addition to these challenges of interpretation and visibility at fluvial archaeological sites, geochronological methods are needed to establish the timing of deposition of different sedimentary packages and to develop conceptual models of site formation (e.g., Tooth et al., 2013; Lyons et al., 2014). Radiocarbon provides a valuable method back to ~40 ka, but beyond this range it is commonly difficult to provide a numerical chronology. However, over the last two decades developments in luminescence dating have provided an excellent chronological tool that is now widely applied (Rhodes, 2011). The optically stimulated luminescence (OSL) signal from quartz (Duller, 2004) has been demonstrated to yield accurate ages for alluvial river terrace and other fluvial deposits ranging in age from a few tens of years to in excess of a hundred thousand years (e.g., Rittenour, 2008; Macklin et al., 2010; Lyons et al., 2014), but for many older deposits the OSL signal may be saturated. Beyond the range of quartz OSL methods, cosmogenic burial dating (e.g., Gibbon et al., 2009; Erlanger et al., 2012), biostratigraphy (e.g., Schreve et al., 2002), electron spin resonance (Rosina et al., 2014), and relative dating methods such as amino

acid racemization (e.g., Penkman et al., 2011) have been applied to fluvial deposits, but in many cases the resolution of ages is limited.

This paper combines luminescence dating of deposits in the central Kalambo Basin with new geomorphological and sedimentological insights to propose a conceptual model outlining the key fluvial processes involved in site formation. It then discusses the implications of this model for the generation, preservation, and visibility of the archaeological record. Barham et al. 2015 provides details of the artefacts recovered during these excavations, as well as additional sedimentological and palaeoenvironmental information.

2. Previous chronological investigations at Kalambo Falls

A number of different geochronological methods have previously been used on material collected from Kalambo Falls, but with only limited success for the pre-Holocene. Samples of organic-rich clays and some scattered charcoal were collected for radiocarbon dating during Clark's excavations in the 1950s and 1960s. By applying enrichment techniques at the Groningen Radiocarbon Laboratory, finite ages up to 60 ka BP were obtained from Acheulean levels in site A (Sheppard and Kleindienst, 1996; Clark, 2001). Although enrichment of these samples provided radiocarbon measurements that were above instrumental background, the techniques are not able to overcome contamination arising during burial. Less than 0.1% of contamination by modern carbon would result in a sample that is hundreds of thousands of years old, giving an apparent radiocarbon age of 60 ka BP (Taylor, 1987), and the radiocarbon ages obtained for material from Kalambo are all thought to underestimate the true age of the site (Sheppard and Kleindienst, 1996; Clark, 2001).

An unusual feature of the Kalambo Falls site is the preservation in sites A and B of wood in the Sangoan and Acheulean levels as a

result of waterlogging of the deposits (Clark, 2001). This wood has been the subject of two attempts to provide a numerical chronology. Lee et al. (1976) used the racemization of proline and hydroxyproline in the wood to estimate a minimum age of 110 ka. McKinney (2001) applied uranium-series methods to wood samples attributed to the Sangoan, Acheulean Upper level, and Acheulean Lower level, leading to isochron ages of 76 ± 10 ka, 182 ± 10 ka, and 182 ± 16 ka, respectively. However, uranium series methods are rarely applied to wood. The occurrence of U in fossil wood in sufficient concentrations to make uranium-series methods possible implies that uranium migrated into the system after deposition, but it is difficult to be confident that the system has been geochemically closed since this initial input of uranium, and hence the ages may be unreliable.

In short, the chronology of the Kalambo Falls site is poorly known. Clark (2001) recognised the potential contribution of luminescence dating to improve the chronology, but only with recent developments in the suite of luminescence techniques, especially as applied to fluvial deposits containing quartz-rich sand, has there been an opportunity to fulfil this potential and thus reassess the significance of the Kalambo Falls archaeological record.

3. Methods

3.1. Field sampling

Re-examination of the Kalambo Falls archaeological site was undertaken in 2006 (Barham et al., 2009) and involved four unit excavations at Site C North (S8°35′31.01″; E31°14′33.37″), located on a 5−7 m tall bank section immediately north of the original Site C of Clark (1969). From south to north, the excavations were designated C, C3, C1, and C2 (Figs. 1c and 2).

A total of 18 samples (KB1-KB17 and KB19) were collected from the four excavations for luminescence dating (Fig. 2). Sample locations were selected to establish the timing of major breaks in the sedimentary succession and to bracket key archaeological horizons, especially those associated with Mode 2 and Mode 3 artefacts (Fig. 2). Care was taken to avoid sampling within 20 cm of major sedimentary boundaries in order to avoid complexities in the gamma dose rate. Wherever possible, layers containing abundant sand were targeted, and samples were collected by hammering 5 cm diameter opaque plastic tubes into freshly excavated faces or

by directly collecting sediment into black plastic bags under a light-tight plastic sheet. The ends of any sample tubes were packed with plastic to prevent movement of sediment inside the tube and then sealed to allow transport back to the laboratory. For each sample, with the exception of KB11, in situ measurement of the gamma dose rate was made using a portable gamma spectrometer (Ortec MicroNomad equipped with a 2 inch diameter NaI crystal).

3.2. Laboratory procedures

To determine an age using luminescence methods requires measurement of two parameters, the equivalent dose (D_e) and the dose rate (D_r; Duller, 2008a). The D_e is the radiation dose received by the sample since the event being dated and is measured by making luminescence measurements of the sample. D_e has the SI unit of Grays (Gy), where 1 Gy is equivalent to an energy of 1 J/kg being absorbed by the sample. When dating the deposition of sediments, the event being dated is the last exposure of the sediment mineral grains to daylight, as this bleaching reduces the D_e to a very low level. The D_r is the rate at which the sample is exposed to ionizing radiation in the natural environment and has the units Gy per thousand years (Gy/ka). The age is calculated by dividing D_e by D_r (Duller, 2004, 2008a). Over the past two decades, measurement of the optically stimulated luminescence (OSL) signal from quartz has been applied widely to provide ages for deposits from a few years to in excess of 100 ka (Murray and Olley, 2002). The method has played an increasingly important role in providing an absolute chronology for Middle Stone Age archaeological sites around the world, including India (e.g., Petraglia et al., 2007), Arabia (e.g., Armitage et al., 2011), southern Africa (e.g., Jacobs et al., 2008), and northern Africa (e.g., Clark-Balzan et al., 2012). OSL has proved especially important in providing ages for sites that lie beyond the range of radiocarbon, and where tephra are not found.

Expanding our knowledge of the Mode 2 to Mode 3 transition and the broader sequence of changes in the Kalambo Basin is dependent on being able to place recovered artefacts in an absolute chronological framework. Whilst quartz OSL has played a valuable role in constraining events within the MSA, it may be of limited value in dating older sites. The upper age limit possible using quartz OSL measurements varies from one sample to another (Duller, 2008a) but is commonly in the range of 100−150 ka. At certain sites, it is possible to use quartz OSL to calculate older ages because
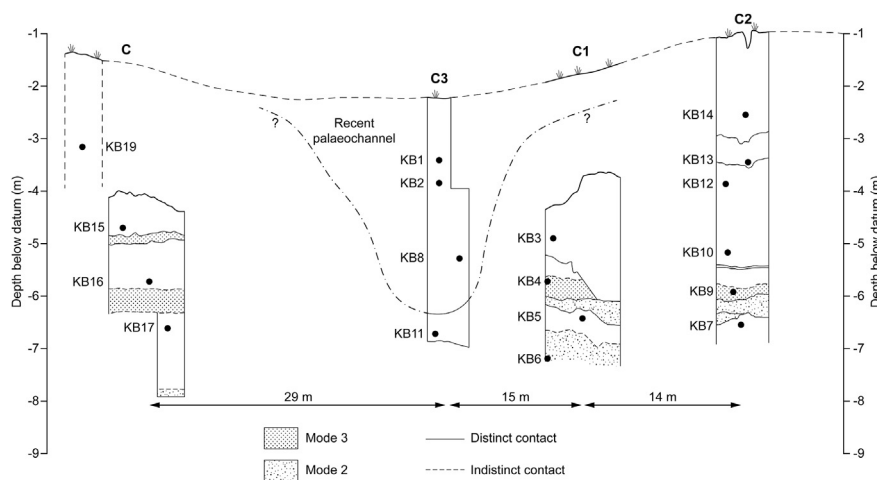
Figure 2. Simplified stratigraphy exposed in the excavations at Site C North in the central Kalambo Basin, indicating the major stratigraphic boundaries, the archaeological horizons, and luminescence sample locations. Detailed sedimentological logs for Units C, C1, and C2 are provided in Barham et al. (2015). The horizontal distance between units is indicated at the bottom of the diagram.

the dose rate (D$_r$) is unusually low. For example at Kathu Pan, Porat et al. (2010) were able to obtain an age of 291 ± 45 ka because the dose rate was extremely low (0.47 ± 0.07 Gy/ka). However, even with the low dose rates found at this site, the lowermost sample (464 ± 47 ka) in the study was near the limit of OSL, and it was the correspondence with ESR measurements that increased the likelihood that this OSL age was reliable. To provide a chronology extending back to the ESA/MSA transition, new luminescence methods are required. The thermally transferred OSL (TT-OSL) signal from quartz (Duller and Wintle, 2012) is one potential signal that has been explored and is applied here in combination with quartz OSL.

3.2.1. *Sample processing* All sample processing and analysis was undertaken in Aberystwyth Luminescence Research Laboratory. Standard preparation procedures were followed to separate sand-sized grains of quartz for luminescence measurements. Organic material and carbonates were removed by immersing the samples in 10% H_2O_2 and then 10% HCl until no subsequent reaction was observed. After drying, the samples were sieved to obtain grains ranging from 180–212 μm or 180–250 μm in diameter depending upon the availability of material. Solutions of sodium polytungstate at densities of 2.62 and 2.70 g/cm^3 were then used to remove the majority of feldspars and heavy minerals. Grains with a density between these two values were then subject to etching in 40% hydrofluoric (HF) acid for 45 min. This treatment served two purposes: first, to dissolve any remaining feldspar grains, and second, to etch away the outer ~10 μm of the quartz grains and thus remove the alpha irradiated layer. After rinsing in concentrated HCl to ensure that no fluorides were precipitated, the grains were then resieved to remove grains with a diameter less than 180 μm, with the aim of removing any remaining feldspar fragments that had survived the HF etching.

3.2.2. *Dosimetry measurements* Assessing the radiation dose rate to which samples were exposed during burial (D$_r$) is a crucial part of luminescence dating. For the samples from Kalambo Falls, three sets of measurements were made. At the time of collection, an Ortec MicroNomad portable gamma spectrometer was inserted into the sample holes left after collection of the luminescence samples. A gamma spectrum was collected, permitting both an assessment of the concentration of U, Th, and K and an assessment of the total gamma dose using the threshold method (Mercier and Falgueres, 2007). In the laboratory, a dried subsample of the material collected for each luminescence sample was milled to a fine powder and homogenised. This powdered subsample was then measured using two emission counting methods, thick source alpha counting (TSAC) and beta counting (using a GM-25 beta counter).

The consistency of the data collected by these three methods was assessed by comparing the values calculated for the beta and gamma dose rates using different methods. The beta dose rate measured directly using the GM-25 beta counter was compared with the beta dose rate calculated using the estimates of U, Th, and K concentrations derived from the field gamma spectrometry (Fig. 3a). All values fall close to the 1:1 line, with the exception of sample KB4 for which the beta dose rate measured in the laboratory (2.64 ± 0.08 Gy/ka) is more than double that calculated from the field gamma spectrometry measurements (1.21 ± 0.02 Gy/ka). A similar situation is observed when comparing gamma dose rates determined from field measurements using the threshold method with the gamma dose rate calculated from laboratory TSAC and beta counting (Fig. 3b). All samples lie close to the 1:1 line, but the gamma dose rate for KB4 (not shown) determined in the field is 1.26 ± 0.04 Gy/ka, while that from laboratory measurements is 3.39 ± 0.15 Gy/ka. There is a clear discrepancy between the field
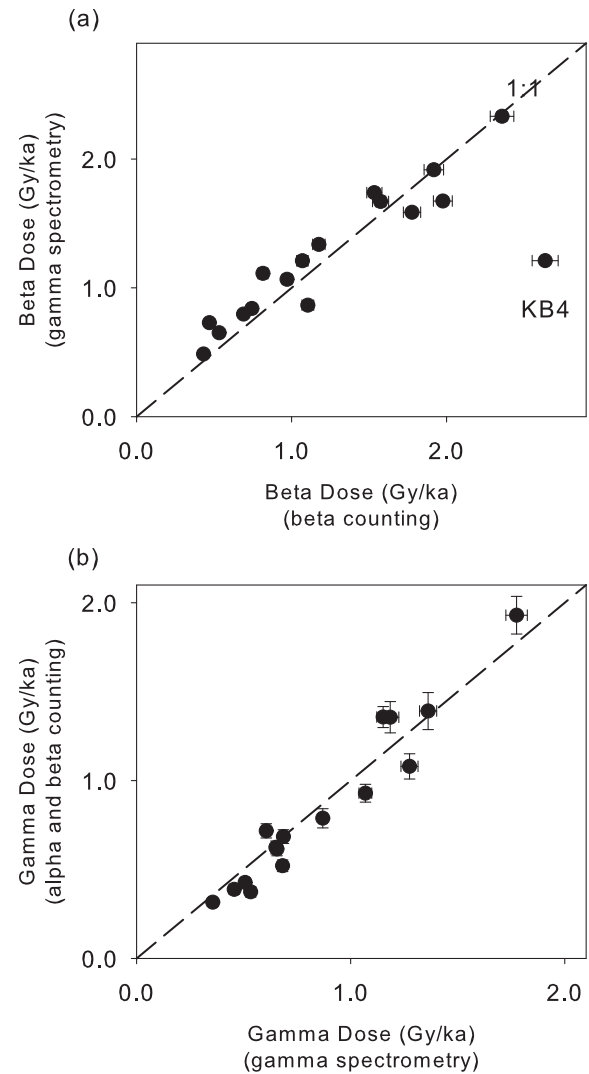
Figure 3. Comparison of beta and gamma dose rates derived using different dosimetry methods for the samples dated in this study.

based and laboratory based measurements of dose rate for KB4. In the part of Unit C1 below where KB4 was collected, mud balls up to 10 cm in diameter were observed within the sandy matrix. The selection of sites for OSL sampling aimed to avoid such complex stratigraphy, but the tube used to sample KB4 inadvertently passed through one of these mud balls, and caused this discrepancy between the dose rates measured in situ and in the laboratory (Fig. 3).

The dose rates used for age calculation are shown in Table 1. The beta dose rate was calculated using the GM-25 beta counter data, and the gamma dose rate using in situ gamma spectrometry calculated using the threshold method. The advantage of these methods is that they directly measure the beta and gamma dose received by the sample, rather than making any assumptions about homogeneity in the dose rate over different spatial scales. For KB4, this makes the assumption that the dosimetry sample measured in the laboratory accurately represents the dosimetry of the part of the sample used to separate quartz for OSL measurements.

The beta dose rate was corrected for grain size attenuation, and both the beta and gamma dose rates were corrected for water content. Water content for these samples varies depending upon their stratigraphic position. Geomorphological field evidence suggests that samples near the base of the excavated units will have

Table 1
Dosimetry data for luminescence samples collected at Kalambo Falls[a].

Sample	Depth below surface (m)	Water content (%)	Grain size (μm)	Beta dose (Gy/ka)	Gamma dose (Gy/ka)	Cosmic dose (Gy/ka)	Total dose (Gy/ka)
Unit C							
KB19	1.75	10 ± 5	180–212	0.76 ± 0.05	0.59 ± 0.04	0.169 ± 0.009	1.516 ± 0.061
KB15	3.25	15 ± 5	180–250	0.55 ± 0.04	0.43 ± 0.03	0.141 ± 0.007	1.120 ± 0.045
KB16	4.30	15 ± 5	180–250	0.39 ± 0.03	0.39 ± 0.02	0.125 ± 0.006	0.905 ± 0.034
KB17	5.17	20 ± 5	180–250	0.30 ± 0.02	0.29 ± 0.02	0.114 ± 0.006	0.705 ± 0.026
Unit C1							
KB3	3.10	10 ± 5	180–212	0.92 ± 0.06	0.78 ± 0.05	0.144 ± 0.007	1.843 ± 0.077
KB4	3.65	15 ± 5	180–212	1.95 ± 0.12	1.07 ± 0.06	0.135 ± 0.007	3.158 ± 0.136
KB5	4.25	15 ± 5	180–250	0.34 ± 0.02	0.46 ± 0.03	0.123 ± 0.006	0.918 ± 0.036
KB6	5.25	20 ± 5	180–250	0.49 ± 0.03	0.53 ± 0.03	0.113 ± 0.006	1.124 ± 0.043
Unit C2							
KB14	1.45	10 ± 5	180–212	1.20 ± 0.08	1.15 ± 0.07	0.175 ± 0.009	2.518 ± 0.103
KB13	2.35	10 ± 5	180–212	1.39 ± 0.09	1.06 ± 0.07	0.157 ± 0.008	2.608 ± 0.111
KB12	2.88	15 ± 5	180–212	1.74 ± 0.11	1.52 ± 0.09	0.147 ± 0.008	3.407 ± 0.138
KB10	4.03	15 ± 5	180–212	1.16 ± 0.07	0.91 ± 0.05	0.129 ± 0.007	2.206 ± 0.089
KB9	4.73	20 ± 5	180–212	0.75 ± 0.05	0.56 ± 0.03	0.119 ± 0.006	1.430 ± 0.055
KB7	5.46	20 ± 5	180–212	0.78 ± 0.05	0.49 ± 0.03	0.110 ± 0.006	1.380 ± 0.055
Unit C3							
KB1	1.25	10 ± 5	180–212	1.54 ± 0.10	1.03 ± 0.06	0.179 ± 0.009	2.756 ± 0.115
KB2	1.70	10 ± 5	180–212	0.64 ± 0.04	0.61 ± 0.04	0.170 ± 0.009	1.418 ± 0.056
KB8	3.05	15 ± 5	180–212	1.42 ± 0.09	1.16 ± 0.07	0.144 ± 0.007	2.727 ± 0.110
KB11	4.50	20 ± 5	180–250	0.41 ± 0.03	0.35 ± 0.03	0.122 ± 0.006	0.882 ± 0.041

[a] Beta and gamma dose rates listed have been corrected for the effect of water content and grain size.

been saturated, while lower average values are likely higher in the succession. Values varying from 20 ± 5% at the base to 10 ± 5% at the top of the units were used, with these values being based on estimates of the saturated water content made in the laboratory and measurements of the water content of the samples at the time of collection. The dose rate due to cosmic rays was calculated using the equations in Prescott and Hutton (1994) and assuming the current thickness of overburden.

3.2.3. Luminescence equipment All luminescence measurements were made on Risø automated luminescence readers (TL-DA-15; Bøtter-Jensen et al., 2003). Optical stimulation of single grains was achieved using a 532 nm Nd:YVO$_4$ laser, focused so that it could be directed onto a single ~200 μm diameter grain of quartz. Single grain measurements were either made for 1 s duration using 90% of the laser power, or 4 s duration using the laser at 25% of full power. This latter setting was used for the majority of the measurements reported here in order to give greater detail in the measurement of the OSL decay curves. An instrumental uncertainty of 2% has been included in the analysis of all single grain data. Further details of this equipment and the advantages of single grain measurements are given in Bøtter-Jensen et al. (2003), Jacobs and Roberts (2007), and Duller (2008b).

Stimulation of the TT-OSL signals was achieved using blue light emitting diodes (470Δ20 nm). Luminescence emissions (both OSL and TT-OSL) were measured using EMI 9635QA photomultiplier tubes fitted with 7.5 mm thickness of Hoya U-340 glass filters. The Risø readers were equipped with Sr/Y beta sources for laboratory irradiation, and these were calibrated against a secondary international standard in Denmark.

4. Results

### 4.1. Single grain optically stimulated luminescence (OSL) measurements

All 18 of the samples collected from Site C North were deposited by fluvial processes associated with the Kalambo River. Previous work has demonstrated that in some fluvial settings the OSL signal in quartz may not be completely reset to zero at deposition and that

a residual remains, leading to the potential for luminescence ages to be overestimated (Rittenour, 2008). This incomplete bleaching is important for young samples, where the residual is large compared with the dose accumulated during burial. For older samples, this residual becomes less important (Jain et al., 2004).

Single grain OSL dating can be used to test explicitly whether a sample is affected by incomplete bleaching at deposition, and this method has been applied here. The single aliquot regenerative (SAR) dose method has been used to measure equivalent dose (D_e), with a preheat of 240 °C for 10 s and a cutheat of 220 °C for the test dose. Screening of the data was undertaken so that only those grains that had appropriate luminescence characteristics were used for dating. The acceptance criteria are those described in Duller (2012), based on those previously described by Jacobs et al. (2006). Fig. 4 shows the OSL decay curve from a single grain of quartz from sample KB15 that passes all these criteria, along with the SAR dose response curve generated for this grain.

Duller (2012) undertook a series of dose recovery experiments on sample KB15 using these measurement parameters and demonstrated that excellent dose recovery can be achieved up to doses of approximately 95 Gy. Above this dose, saturation of the OSL signal leads to increasing difficulty in accurately recovering a laboratory administered dose. All 18 samples have had single grain measurements made upon them, although for some samples the natural OSL signal of many of the grains is saturated. A large proportion (24%) of the quartz grains from Kalambo Falls yield an OSL signal suitable for constructing a dose response curve, and between 800 and 2000 grains from each sample have been measured (Table 2). The single grain dose distributions observed for these samples fall into three categories: (1) those affected by incomplete bleaching; (2) those that can best be modelled assuming a single dose population; and (3) those affected by saturation of the OSL signal. These are discussed in turn below.

4.1.1. Samples affected by incomplete bleaching Based on geomorphological observations (see below and Barham et al., 2015), Unit C3 was excavated in a relatively young channel cut-and-fill feature, with samples KB1, KB2, and KB8 collected within the fill (Fig. 2). Fig. 5 shows radial plots of the single grain D_e
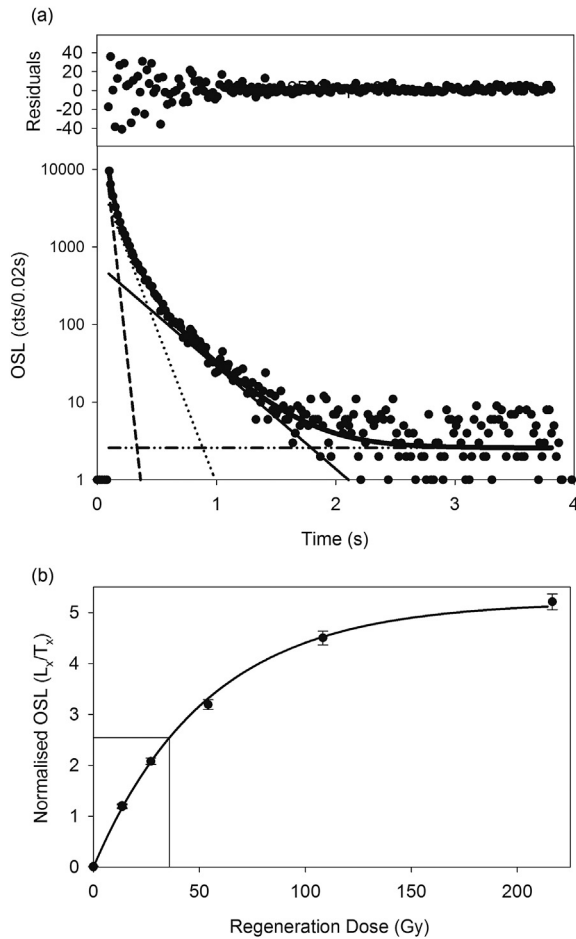
Figure 4. a) OSL decay curve for a single grain of quartz from sample KB15. The decay curve has been fitted with the sum of three exponentials, representing the fast, medium, and slow components of the quartz OSL signal. b) The dose response curve generated for this grain of quartz. The lowest dose point was measured three times; the first two measurements were used to calculate the recycling ratio (0.99 ± 0.04) and the third measurement was made after exposing the grain to infrared stimulation so that an IR depletion ratio (1.02 ± 0.04) could be measured. The equivalent dose (D_e) is 35.9 ± 1.8 Gy.

values obtained for these samples. In all cases, there is a wide range of D_e values. The distribution of D_e values observed in samples KB1 and KB2 at the top of the sequence is typical of what has been observed from other young fluvial deposits (Rodnight et al., 2005). The majority of the grains give a D_e of ~1.3 Gy (KB1) and ~1.0 Gy (KB2) and then a small proportion of grains give much larger D_e values up to ~20 Gy, consistent with the idea that these grains were not exposed to sufficient light at deposition to reset the OSL signal. Sample KB8 was collected 30 cm above the erosional base of the feature, and the D_e distribution for this sample (Fig. 5c) suggests that a much smaller proportion of the grains were exposed to sufficient daylight prior to deposition. For all three samples, the minimum age model (MAM; Galbraith et al., 1999) was applied to determine the appropriate estimate of equivalent dose (D_e) to use for age calculation. These D_e values are given in Table 2 and are shown by a grey bar on each of the radial plots in Fig. 5. Only one other sample has a similar distribution, and this is KB14 near the top of Unit C2 (Fig. 5d). The distribution is very similar to KB8 in that only a small proportion of grains appear to have had their OSL signal reset at the time of deposition. The MAM was applied to this sample as well (Table 2).

4.1.2. Samples dominated by a single dose population

Fig. 6 shows the single grain dose distributions for four samples (KB19, KB15, KB3, and KB9). These samples differ from those shown in Fig. 5 in three main respects. First, KB19, KB15, KB3, and KB9 have D_e values that are on average much higher than those shown in Fig. 5; use of the central age model (CAM) gives values of 58.4 ± 1.2 Gy, 44.1 ± 1.4 Gy, 61.5 ± 1.4 Gy, and 62.5 ± 1.6 Gy, respectively. Second, the dose distributions for the samples shown in Fig. 6 do not appear asymmetric as do KB1, KB2, KB8, and KB14. Finally, the overdispersion (OD) values for KB19, KB15, KB3, and KB9 are in the range 30–33%, while the younger samples have values between 74 and 110% (Table 2).

The average characteristic saturation dose (D_0) for KB15 measured by Duller (2012) was 47 Gy. The calculated CAM D_e values for these four samples are below the threshold of two times the value of D_0 suggested by Wintle and Murray (2006) and supported by the dose recovery data of Duller (2012) and the measurements of Chapot et al. (2012). This observation, along with the lack of asymmetry in the dose distributions gives confidence that the CAM D_e values given in Table 2 for these four samples are reliable estimates to use for age calculation.

4.1.3. Samples affected by saturation of the quartz OSL signal

The remaining 10 samples (listed in the same order as they appear in the tables: KB16, KB17, KB4, KB5, KB6, KB13, KB12, KB10, KB7, and KB11) may be affected by saturation of the OSL signal. To illustrate this problem, Fig. 7 shows the dose response curve for a single grain of quartz from sample KB16. The natural signal measured from this grain is at, or above, the asymptotic value determined from laboratory regeneration measurements. Thus, it is not possible to determine a D_e for this grain, and it is saturated. Grains were defined as saturated if the normalised natural OSL signal was above the asymptotic value for the dose response curve or if one of the error margins was above this value. The impact of saturation becomes increasingly apparent as older samples are analysed. Fig. 8 shows the percentage of grains that give a D_e value as a function of dose. Duller (2012) showed in laboratory measurements that as the given dose increased from 50 to 170 Gy the proportion of grains which gave a D_e decreased from almost 100% to approximately 50%. For some of the samples analysed from Kalambo Falls, 25% of grains or less gave D_e values. The comparison shown in Fig. 8 is made difficult because the dose received by samples in nature is unknown, and the large proportion of grains that are saturated suggests that the calculated D_e may be underestimated.

While the CAM D_e calculated for some samples is almost certainly affected by saturation (e.g., KB7, where only 14% of grains give a D_e), the impact on other samples is more difficult to assess. For instance, samples KB13, KB12, and KB10 have CAM D_e values between 79.0 and 82.1 Gy, overdispersion values of 28–36%, and between 48 and 52% of grains give D_e values. These samples give CAM D_e values that are less than twice the value of D_0, but it is unclear from this single grain data alone whether these CAM D_e values are reliable or whether they are minimum values. For this reason, TT-OSL measurements were undertaken to attempt to overcome saturation of the OSL signal.

4.2. Thermally transferred optically stimulated luminescence (TT-OSL) measurements

TT-OSL is a signal that has been explored in quartz in recent years (Duller and Wintle, 2012). It has been applied in a small number of archaeological settings to extend the age range over which luminescence dating methods can be applied (e.g., Kim et al., 2010; Arnold et al., 2014). The principal advantage of TT-OSL over the more commonly used OSL signal is the dose response characteristic (Fig. 9), which shows continued growth of the signal at

Table 2
Single grain OSL equivalent dose data and ages for samples collected at Kalambo Falls[a].

| Sample	Number of grains			OD (%)	Age model	Equivalent dose (Gy)	Dose rate (Gy/ka)	Age (ka)
	Measured	Pass all criteria	Give D_e					
Unit C								
KB19	1200	407	306 (75%)	33	CAM	58.4 ± 1.2	1.516 ± 0.061	38.5 ± 1.7
KB15	800	128	110 (86%)	31	CAM	44.1 ± 1.4	1.120 ± 0.045	39.4 ± 2.0
KB16	1000	172	53 (31%)	54	CAM	>123 ± 9.9	0.905 ± 0.034	>136 ± 12
KB17	1000	196	71 (36%)	52	CAM	>117 ± 7.8	0.705 ± 0.026	>166 ± 13
Unit C1								
KB3	1200	297	246 (83%)	32	CAM	61.5 ± 1.4	1.843 ± 0.077	33.4 ± 1.6
KB4	1000	197	39 (20%)	67	CAM	>98 ± 11	3.158 ± 0.136	>31.0 ± 3.7
KB5	1000	202	60 (30%)	50	CAM	>140 ± 10	0.918 ± 0.036	>152 ± 12.4
KB6	1000	275	86 (31%)	59	CAM	>146 ± 10	1.124 ± 0.043	>130 ± 10.1
Unit C2								
KB14	1900	597	597 (100%)	110	MAM	1.68 ± 0.05	2.518 ± 0.103	0.67 ± 0.03
KB13	2000	476	247 (52%)	28	CAM	>80.8 ± 1.7	2.608 ± 0.111	31.0 ± 1.5
KB12	2000	490	234 (48%)	36	CAM	>82.1 ± 2.2	3.407 ± 0.138	24.1 ± 1.2
KB10	1900	413	214 (52%)	28	CAM	>79.0 ± 1.8	2.206 ± 0.089	35.8 ± 1.7
KB9	1000	205	169 (82%)	30	CAM	62.5 ± 1.6	1.430 ± 0.055	43.7 ± 2.0
KB7	1000	185	26 (14%)	61	CAM	>121 ± 16	1.380 ± 0.055	>87.7 ± 12.1
Unit C3								
KB1	1000	243	243 (100%)	74	MAM	1.34 ± 0.05	2.756 ± 0.115	0.49 ± 0.02
KB2	1100	283	283 (100%)	93	MAM	1.04 ± 0.02	1.418 ± 0.056	0.73 ± 0.03
KB8	1000	369	360 (98%)	76	MAM	3.86 ± 0.21	2.727 ± 0.110	1.42 ± 0.10
KB11	900	199	88 (44%)	90	CAM	>98.9 ± 9.8	0.882 ± 0.041	>112 ± 12

[a] All ages are reported in thousands of years (ka) before the date of measurement (AD 2010). Where the MAM was used, an overdispersion value of 15% was assumed for the model.
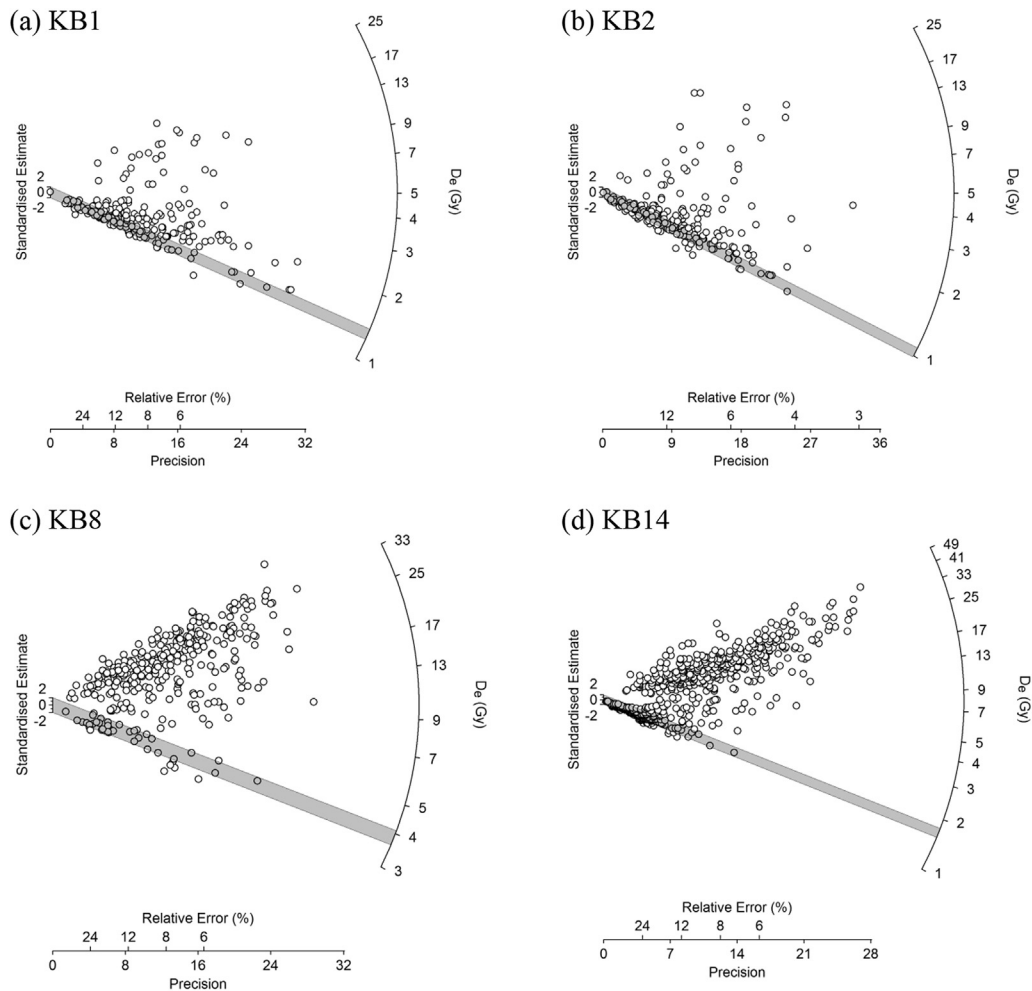
Figure 5. Radial plots of equivalent dose data for four samples where incomplete bleaching is significant: a) KB1; b) KB2; c) KB8; and d) KB14.
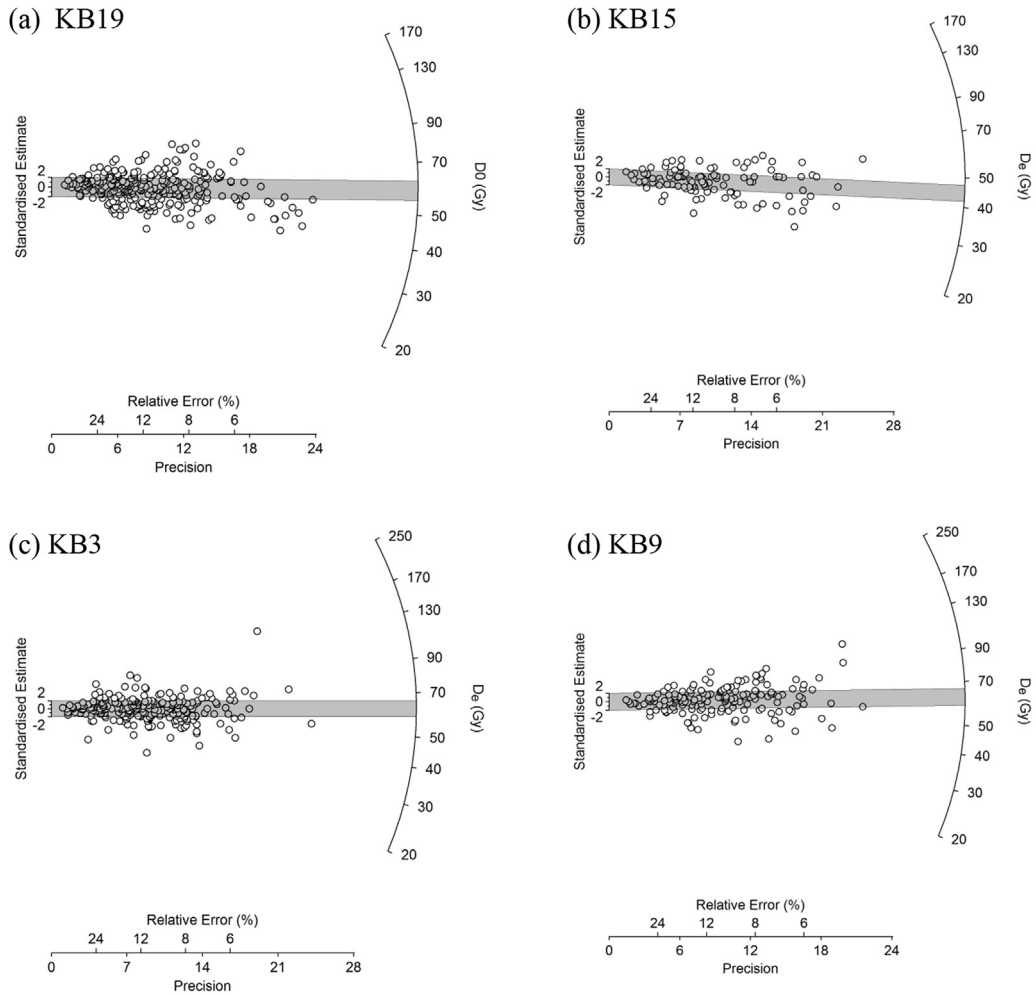
Figure 6. Equivalent dose distributions for four samples dominated by a single population: a) KB19; b) KB15; c) KB3; and d) KB9.

much higher doses than is observed for the OSL signal. However, the TT-OSL signal is normally at least one hundred times weaker than the OSL signal (Duller and Wintle, 2012). Initial experiments on samples from Kalambo Falls attempted to measure TT-OSL from single grains of quartz, but signal levels were too low. Thus, all measurements of the TT-OSL signal reported here were made on medium sized aliquots (consisting of ~ 500 grains of quartz) in order to obtain a sufficiently strong signal.
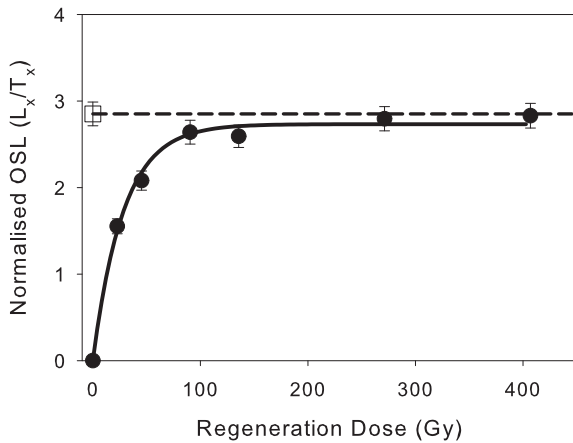
Figure 7. Dose response curve for the OSL signal from a single grain of quartz from sample KB16. The open square and the dashed horizontal line show the natural signal. The dose response curve determined from laboratory regeneration doses does not intersect with the natural signal, demonstrating that the natural OSL signal in this grain had reached saturation.
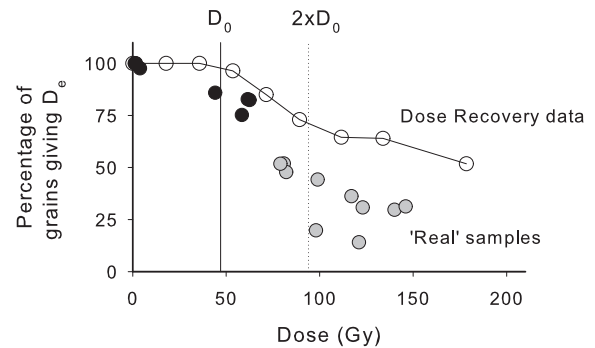
Figure 8. The percentage of grains that pass all appropriate selection criteria (e.g., recycling, IR-OSL ratio, recuperation) which give an equivalent dose (D_e) value. At higher doses, a decreasing percentage of grains yield a D_e value because the OSL signal is saturated. Two datasets are shown. The first is dose recovery data (white circles) for sample KB15 from Duller (2012) and the x-axis is the known dose administered in the laboratory. The second is for the suite of 18 samples reported in this paper and the x-axis is the estimate of equivalent dose based on OSL measurements. For this second dataset, samples shown in black are finite values, while for those in grey the D_e may be a minimum value because of saturation. Values of D_0 and twice the value of D_0 are taken from Duller (2012).
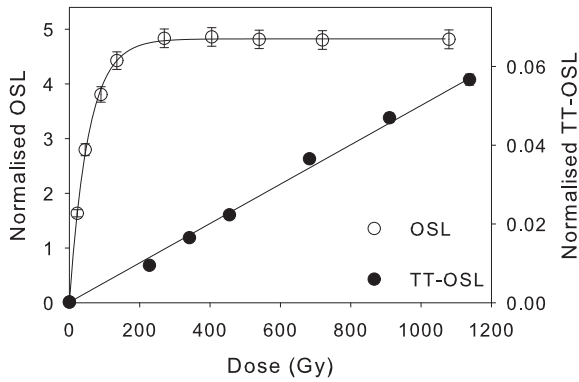
Figure 9. Dose response curves for two luminescence signals from quartz grains of sample KB7. Single grain OSL measurements show the onset of saturation in the first 150–200 Gy, while the TT-OSL signal (derived from a multiple grain aliquot) shows a linear growth in signal up to 1000 Gy.

The single aliquot regenerative (SAR) dose protocol developed by Adamiec et al. (2010) was used for all TT-OSL measurements in this study. This protocol holds the aliquot at 350 °C for 200 s at the end of each SAR cycle in order to remove any charge remaining in the TT-OSL defect and thus improves recycling. The effectiveness of this protocol was tested by undertaking a dose recovery experiment on sample KB1. Sixteen aliquots were used, with eight receiving no treatment and eight receiving a known laboratory beta dose of 182 Gy prior to any other treatment. All sixteen aliquots then had their D_e measured using the Adamiec et al. (2010) TT-OSL SAR protocol. After subtracting the residual dose in KB1 (discussed below), the ratio of the given to the recovered dose was 0.97 ± 0.09, demonstrating that it was possible to accurately measure the known laboratory radiation dose.

One of the drawbacks of the TT-OSL signal is that it is reset by daylight much more slowly than the quartz OSL signal (Jacobs et al., 2011; Duller and Wintle, 2012), and hence most previous applications of this method have been on aeolian samples. The single grain OSL data for the youngest samples from Kalambo

Falls (e.g., Fig. 5) show that not all grains have been exposed to daylight sufficiently to reset their OSL signal, and thus it would be expected that there would be a large residual TT-OSL signal at deposition. Eight aliquots of each of the two youngest samples (KB1 and KB2) from the channel cut-and-fill feature in Unit C3 (Fig. 2) had their D_e measured using the TT-OSL SAR protocol. When the data from these two samples are combined, they give an average residual dose of 111 ± 5.6 Gy. This TT-OSL residual is larger than that typically measured in aeolian environments (e.g., Tsukamoto et al. (2008) measured 17 Gy in coastal dunes in South Africa and similar values are summarised from the literature in Duller and Wintle (2012)), but smaller than those found for fine grained overbank deposits from the Yellow River in China (259 ± 108 and 282 ± 38 Gy; Hu et al., 2010). Although the values measured for KB1 and KB2 are large, the D_e values for the two samples are very reproducible (both have overdispersion values less than 10%) and are similar to each other (102 ± 10 Gy and 115 ± 6.4 Gy, respectively). The depositional environment for all of the OSL samples collected here is thought to be similar, and therefore it is assumed that this residual dose should be subtracted from the D_e values obtained for all samples from Site C North.

For each sample, eight medium sized aliquots were measured using the SAR TT-OSL protocol. Standard rejection criteria were applied, namely a signal at least three times above the standard deviation of the background, a recycling ratio within 10% of unity, and recuperation less than 5% of the natural. The D_e values measured are listed in Table 3, and the D_e values after subtraction of the 111 ± 5.6 Gy residual are also shown.

One means of checking the veracity of the TT-OSL values is by comparing the D_e values with those obtained using single grain quartz OSL (Fig. 10). For the group of samples shown in Fig. 6 that are dominated by a single population of grains and where saturation is not significant, there is very good agreement between the OSL and TT-OSL D_e values, especially given the large residual dose that has to be subtracted.

Uncertainty about the reliability of the single grain quartz OSL data for samples KB13, KB12, and KB10 was highlighted previously.

Table 3
TT-OSL equivalent dose data and ages for samples collected at Kalambo Falls, and TT-OSL ages corrected for the impact of the lifetime of the charge, assuming a burial temperature of 17 ± 2 °C.

Sample	Dose rate (Gy/ka)	TT-OSL equivalent dose (Gy)	Residual subtracted TT-OSL D_e (Gy)	Uncorrected Age (ka)	Lifetime corrected age (ka)
Unit C					
KB19	1.516 ± 0.061	166 ± 5.2	54.3 ± 7.6	35.8 ± 5.2	36.4 ± 5.5
KB15	1.120 ± 0.045	152 ± 14	40.4 ± 15	36.1 ± 14	36.7 ± 15
KB16	0.905 ± 0.034	446 ± 18	335 ± 19	370 ± 25	455 ± 103
KB17	0.705 ± 0.026	339 ± 24	228 ± 25	323 ± 37	386 ± 94
Unit C1					
KB3	1.843 ± 0.077	164 ± 8.2	52.7 ± 10	28.6 ± 5.5	29.0 ± 5.7
KB4	3.158 ± 0.136	580 ± 37	468 ± 37	148 ± 13	159 ± 17
KB5	0.918 ± 0.036	427 ± 27	316 ± 28	342 ± 33	416 ± 91
KB6	1.124 ± 0.043	473 ± 27	362 ± 28	322 ± 27	384 ± 72
Unit C2					
KB14	2.518 ± 0.103	145 ± 4.3	33.8 ± 7.0	13.4 ± 2.9	13.5 ± 2.9
KB13	2.608 ± 0.111	232 ± 5.7	121 ± 8.0	46.3 ± 3.6	47.3 ± 3.8
KB12	3.407 ± 0.138	201 ± 9.5	89.7 ± 11	26.3 ± 3.4	26.6 ± 3.5
KB10	2.206 ± 0.089	175 ± 6.9	63.3 ± 8.9	28.7 ± 4.2	29.1 ± 4.3
KB9	1.430 ± 0.055	157 ± 5.2	45.4 ± 7.6	31.8 ± 5.5	32.3 ± 5.7
KB7	1.380 ± 0.055	511 ± 22	400 ± 23	290 ± 20	339 ± 49
Unit C3					
KB1	2.756 ± 0.115	102 ± 10	-9.3 ± 12	-3.4 ± 4.2	n/a
KB2	1.418 ± 0.056	115 ± 6.4	4.1 ± 8.5	2.9 ± 6.0	2.9 ± 6.0
KB8	2.727 ± 0.110	140 ± 11	28.4 ± 13	10.4 ± 4.7	10.5 ± 4.8
KB11	0.882 ± 0.041	480 ± 14	369 ± 15	418 ± 26	532 ± 133

(a)

(b)
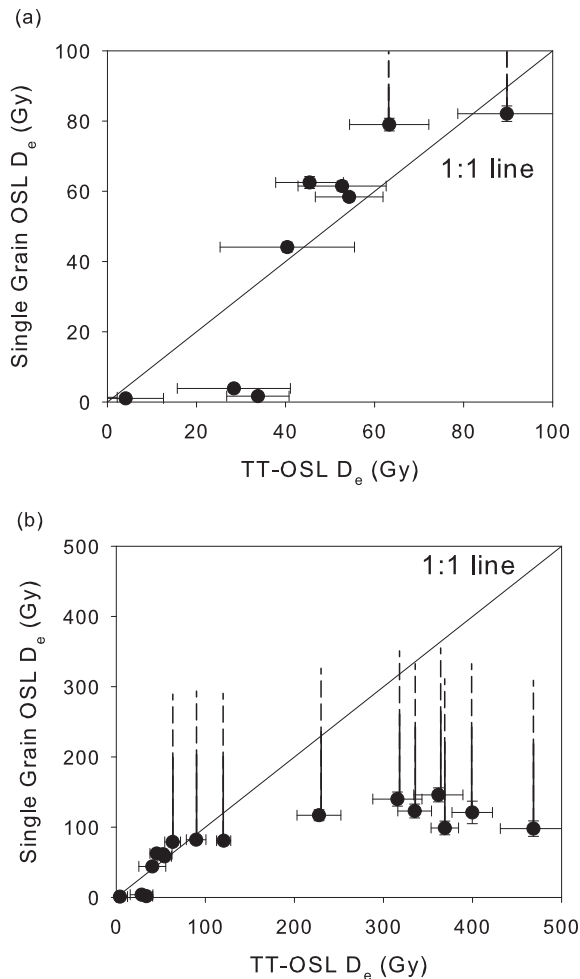
Figure 10. A comparison of equivalent doses calculated for all 18 samples from Kalambo Falls using the OSL signal from single grains of quartz and the TT-OSL signal from medium-sized aliquots. The same data are shown in (a) and (b), but an expanded scale is used in (a) for clarity.

The TT-OSL D_e values (63.3–121 Gy) obtained for these samples are broadly similar to the single grain OSL values (79.0–82.1 Gy), but the two samples (KB4 and KB11) with the next largest single grain OSL D_e values (98 ± 11 and 99 ± 10 Gy, respectively) have TT-OSL D_e values (468 ± 37 and 369 ± 15 Gy) that imply that the quartz OSL is severely affected by saturation. In the case of KB4, the OSL signal of 80% of the grains is saturated, and this differentiates the sample from those where 50% or less of the grains are saturated. However, for KB11, 44% of the grains give D_e values, a proportion that is not very different from those samples where the TT-OSL and single grain OSL D_e values are consistent.

It thus appears that it is difficult to devise criteria by which to assess the reliability of D_e values obtained using the quartz OSL signal from samples as they approach saturation. For this suite of samples, the single grain OSL data appear reliable when the CAM D_e is less than about 70 Gy, and this is also the point at which more than 75% of grains that pass all the acceptance criteria yield D_e values (Table 2). There is then a group of samples where the single grain OSL CAM D_e is about 80 Gy and where about 50% of the grains give D_e values. These values are similar to the TT-OSL D_e values, and thus the OSL appears to be reliable. Given the challenge of measuring the TT-OSL and the need to subtract a substantial residual signal, the OSL ages for samples KB13, KB12, and KB10 are considered more reliable than the TT-OSL ages. For samples where

the single grain OSL CAM D_e is around 100 Gy or higher (KB16, KB17, KB4, KB5, KB6, KB7, KB11), the TT-OSL suggests that these values are strongly affected by saturation of the OSL signal and significantly underestimate the true burial dose. In these cases, TT-OSL provides the most reliable age estimates.

4.2.1. Correcting for the impact of the lifetime of the TT-OSL signal Adamiec et al. (2010) calculated the lifetime of charge in the trap responsible for the TT-OSL signal in quartz based upon laboratory experiments and obtained a value of 4.5 Ma at 10 °C. Thiel et al. (2012) compared ages determined using TT-OSL with those determined using the post-IR IR signal from feldspars, and assuming that the post-IR IRSL ages were correct, they saw underestimation of the TT-OSL ages consistent with the kinetic parameters calculated by Adamiec et al. (2010). It therefore seems that TT-OSL ages require correction for the instability of charge in the trap responsible for the signal. Although this correction is small for samples less than 100 ka, the corrections are larger for samples from near the base of each of the excavation units.

The lifetime of charge in the TT-OSL trap is temperature dependent. The mean annual temperature at Mbala (30 km from Kalambo Falls) based on instrumental records covering the period from 1967 to 1986 is 18.7 °C (NOAA; ftp://ftp.atdd.noaa.gov/pub/ GCOS/WMO-Normals/TABLES/REG__I/ZA/67413.TXT). Over the long time periods (>50 ka) that some of these samples have been buried, temperatures are likely to have been lower on average than present, but the magnitude of cooling in the tropics is poorly constrained. The most relevant data for this part of Africa are the studies by Tierney et al. (2008) and Woltering et al. (2011) who presented TEX_{86} based temperature reconstructions for Lakes Tanganyika and Malawi over the last 60 and 74 ka, respectively. The two temperature constructions are consistent with each other and imply that although temperatures may have varied by as much as 6 °C, the average temperature is likely to be only ~1–2 °C cooler than the present. In order to correct the TT-OSL ages for charge instability, a mean burial temperature of 17 ± 2 °C has been assumed. Using the kinetic parameters of Adamiec et al. (2010), the lifetime of charge in the TT-OSL defect at this temperature is 1.06 Ma. Ages in the final column of Table 3 have been corrected to account for this thermal lifetime using the following equation (based on that given in Adamiec et al., 2010):

$$Age = -\tau \cdot \ln\left(1 - \frac{Age_m}{\tau}\right)$$

where the measured age (Age_m) is corrected for the impact of the lifetime (τ). This approach assumes that growth of the TT-OSL signal is linear during the period being considered, and for the Kalambo samples this is an appropriate assumption (Fig. 9). The lifetime is calculated from the values of trap depth (E), escape frequency (s), and mean annual temperature (T) using the equation:

$$\tau = \frac{1}{s} e^{\left(\frac{E}{kT}\right)}$$

Uncertainties in the corrected ages were determined by incorporating the error on the TT-OSL age and the uncertainty on the burial temperature (17 ± 2 °C) using a Monte Carlo method.

4.3. Luminescence chronology of deposits at Kalambo Falls

Table 4 summarises the luminescence chronology for the four unit excavations at Site C North, and the ages are shown in Figs. 11–14. For the younger samples, which were not affected by saturation, ages derived from single grain OSL measurements have

Table 4
Summary of the luminescence chronology for the four units excavated at Kalambo Falls.

Sample	Signal used	Age Model	Age (ka)
Unit C			
KB19	OSL	CAM	38.5 ± 1.7
KB15	OSL	CAM	39.4 ± 2.0
KB16	TT-OSL	CAM	455 ± 103
KB17	TT-OSL	CAM	386 ± 94
Unit C1			
KB3	OSL	CAM	33.4 ± 1.6
KB4	TT-OSL	CAM	159 ± 17
KB5	TT-OSL	CAM	416 ± 91
KB6	TT-OSL	CAM	384 ± 72
Unit C2			
KB14	OSL	MAM	0.67 ± 0.03
KB13	OSL	CAM	31.0 ± 1.5
KB12	OSL	CAM	24.1 ± 1.2
KB10	OSL	CAM	35.8 ± 1.7
KB9	OSL	CAM	43.7 ± 2.0
KB7	TT-OSL	CAM	339 ± 49
Unit C3			
KB1	OSL	MAM	0.49 ± 0.02
KB2	OSL	MAM	0.73 ± 0.03
KB8	OSL	MAM	1.42 ± 0.10
KB11	TT-OSL	CAM	532 ± 133

been used, while TT-OSL is used for the older samples. The OSL signal is preferred for the younger samples because it bleaches more rapidly by exposure to daylight.

The derived ages are in stratigraphic order, within uncertainties, except for sample KB12 in Unit C2 (Fig. 14), which is discussed later. Across the four unit excavations, there appears to be four sedimentary packages with distinct age ranges. The oldest sedimentary
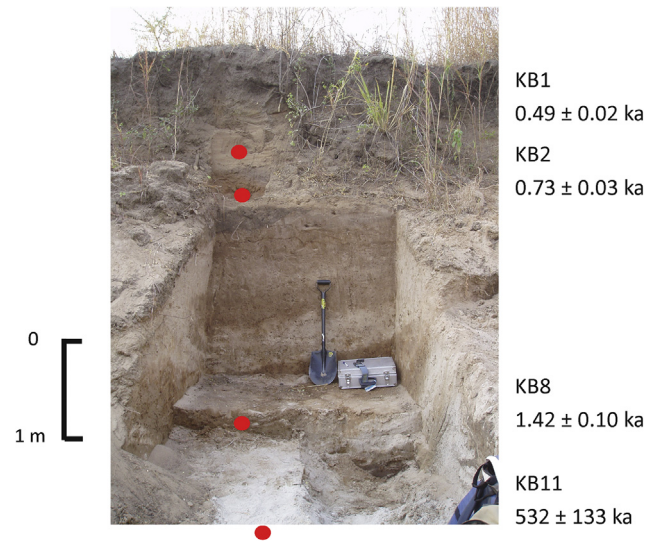

Figure 11. Unit C excavation showing the location of the luminescence samples (red circles) and the ages obtained. Sample KB19 was taken from a small excavation just to the upper left of the main excavation. Scale bar is shown for the front face of the excavation.
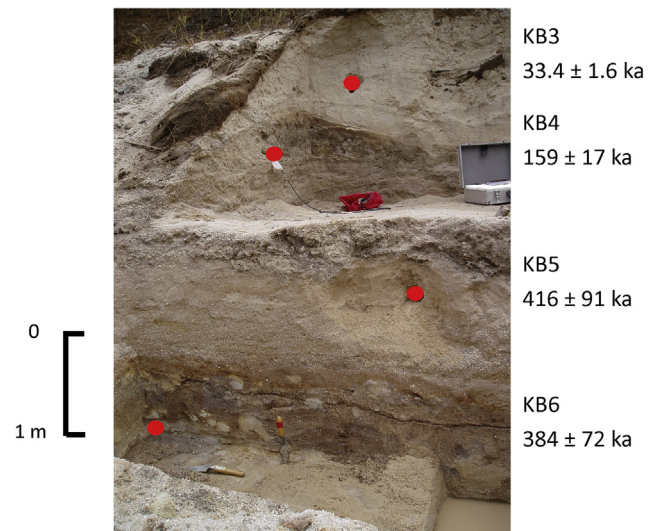
KB19
38.5 ± 1.7 ka

KB15
39.4 ± 2.0 ka

KB16
455 ± 103 ka

KB17
386 ± 94 ka

Figure 12. Unit C3 excavation showing the location of the luminescence samples (red circles) and the ages obtained. Scale bar is shown for the front face of the excavation.

KB1
0.49 ± 0.02 ka

KB2
0.73 ± 0.03 ka

KB8
1.42 ± 0.10 ka

KB11
532 ± 133 ka

package (package 1) is found in the basal parts of all four excavations, with ages ranging from ~500 to 300 ka (Unit C: KB16 and KB17; Unit C1: KB5 and KB6; Unit C2: KB7; Unit C3: KB11). The next youngest sedimentary package (package 2) is poorly preserved, being represented by only a single age in the ~300 to 50 ka range (Unit C1: KB4), and is discussed further below. The next youngest sedimentary package (package 3) is found in three of the units and indicates deposition from ~50 to 30 ka (Unit C: KB 19 and KB 15; Unit C1: KB3; Unit C2: KB13, KB10, and KB9). The youngest sedimentary package (package 4) records deposition from ~1.5 to 0.49 ka and is seen most clearly in Unit C3 (KB1, KB2, and KB8), but is also at the top of Unit C2 (KB14).

Sedimentary package 2 is designated on the basis of the TT-OSL age of 159 ± 17 ka for sample KB4, as this appears to represent a period of deposition distinct from the underlying (package 1) and overlying (package 3) deposits. However, the dosimetry for KB4 was complex, with a large difference between the measurements

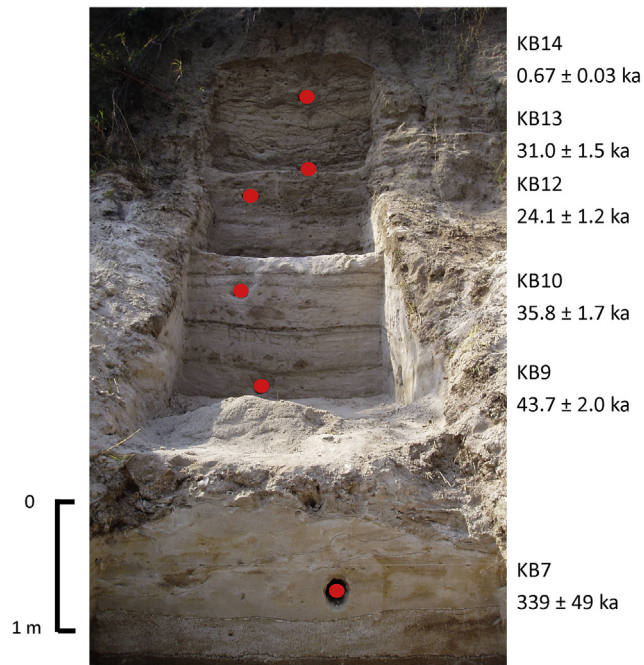**Figure 13.** Unit C1 excavation showing the location of the luminescence samples (red circles) and the ages obtained. Scale bar is shown for the front face of the excavation.

KB3
33.4 ± 1.6 ka

KB4
159 ± 17 ka

KB5
416 ± 91 ka

KB6
384 ± 72 ka

KB14
0.67 ± 0.03 ka

KB13
31.0 ± 1.5 ka

KB12
24.1 ± 1.2 ka

KB10
35.8 ± 1.7 ka

KB9
43.7 ± 2.0 ka

KB7
339 ± 49 ka

0

1 m

Figure 14. Unit C2 excavation showing the location of the luminescence samples (red circles) and the ages obtained. Scale bar is shown for the front face of the excavation.

made in situ and those made in the laboratory (Fig. 3), and the dose rate listed in Table 1 is much higher than for most other samples. The high dose rate observed in the laboratory may be an artefact of having subsampled a clay-rich unit. If only the in situ measurements are used for dosimetry, then the lifetime corrected TT-OSL age for KB4 is 249 ± 33 ka, but this still does not fit within the age ranges for sedimentary packages 1 and 3, as described above.

Sample KB12 (Fig. 14) gives an OSL age (24.1 ± 1.2 ka) that is not consistent with the age of KB13 (31.0 ± 1.5 ka) immediately above. Like KB4, KB12 has a very high dose rate (3.41 ± 0.14 Gy/ka) and it is possible that the discrepancy between this sample and those around it is due to local variations in the dose rate that have not been captured by our dosimetry measurements.

5. Discussion

5.1. Implications of the luminescence chronology for reconstructing fluvial activity at Site C North

Using geomorphological field observations, sedimentological descriptions, and the luminescence ages (Table 4), a model for interpretation of the broad sequence of river and floodplain activity represented in the fluvial succession at Site C North can be proposed (Fig. 15a). As our work focused on the succession in the central part of the Kalambo Basin only, this model should be viewed as a hypothesis that can be tested and perhaps refined using data from other parts of the basin, including at the basin margins where the fluvial succession interfingers with colluvial material (Clark, 2001). Six main stages of river and floodplain activity can be identified, as outlined below.

Stage 1 Between ~500 ka and ~300 ka, the Kalambo River was characterised by lateral migration and minor vertical aggradation, leading to the deposition of relatively coarse-grained (sand, gravel) channel deposits and finer-grained (clay, silt, sand) overbank deposits in the centre of the Kalambo Basin. These deposits represent sedimentary package 1.

Stage 2 Between ~300 ka and 50 ka, the Kalambo River laterally migrated back and forth across the centre of the Kalambo Basin but again with a minor component of vertical aggradation. During lateral migration, channel bed erosion partially truncated the top part of sedimentary package 1 (generally the finer-grained deposits), but younger, relatively coarse-grained channel and finer-grained overbank deposits were deposited. These younger deposits represent sedimentary package 2.

Stage 3 Between ~50 ka and 30 ka, the Kalambo River again laterally migrated back and forth while undergoing minor aggradation. During this stage of lateral migration, channel bed erosion partially truncated or completely removed the top part of sedimentary package 2, so that preservation of this package is spatially patchy (i.e., thin or absent locally) but still younger, relatively coarse-grained channel and finer-grained overbank deposits were deposited. These younger deposits represent sedimentary package 3.

Stage 4 Sometime prior to ~1.5 ka, a small channel—possibly a side branch (floodplain chute) channel of the main Kalambo River—incised partway through the fluvial succession. Rapid refilling of the incised channel with dominantly fine-grained (silt, sand) sediment occurred between ~1.5 and 0.49 ka, with minor fine-grained sedimentation also extending laterally beyond the channel margins atop sedimentary package 3. These young channel fill and overbank deposits represent sedimentary package 4.

Stage 5 After ~0.49 ka, the main Kalambo River incised up to 9 m into the fluvial succession, so that the base and lower banks of the channel were formed in the preserved sedimentary package 1 deposits, and the upper banks were formed in the preserved parts of sedimentary packages 2, 3, and 4.

Stage 6 Following this deep incision, renewed lateral migration is currently occurring at a lower topographic level. Bank erosion, primarily on outer meander bends, is providing new exposures of sedimentary packages 1–4, while concomitant deposition is occurring primarily on inner bends, leading to formation of another package of young deposits in juxtaposition with these older, luminescence-dated, sedimentary packages.

This model provides new insights into the nature, timing, and controls of the river and floodplain processes involved in site formation. Previous studies at Kalambo Falls had identified the punctuated pattern of sedimentation in the basin and had suggested that this could be the result of periodic blocking and unblocking of the spillway gorge through which the Kalambo River flows to reach the falls (e.g., Bond, 1969; Haldemann, 1969; Clark, 2001: 3–4). Our detailed field surveys in August 2006, however, failed to find any unequivocal field evidence to support this hypothesis. On the southern side of the spillway gorge there are rounded and sub-rounded quartzite boulders at high elevations (>5 m) above the current channel. Percussion marks on these boulders may be consistent with fluvial transportation, but these likely relate to much older phases of river activity rather than being evidence for proposed blockage events during the mid or late Pleistocene (Barham et al., 2015). No evidence for truncated debris flows or rockfalls that could have blocked the gorge for extended periods of time were observed. Our model (Fig. 15a) illustrates how the sedimentary packages observed at Site C North could have resulted from ongoing meander dynamics, without necessarily requiring complex interpretations that invoke periodic blocking of the Kalambo River. At present, there is insufficient evidence to clarify the influence of climatic change in each stage of river activity (Barham et al., 2015) but because meander dynamics can occur as an intrinsic part of fluvial activity, climatic forcing is not necessary to explain the observed fluvial succession.
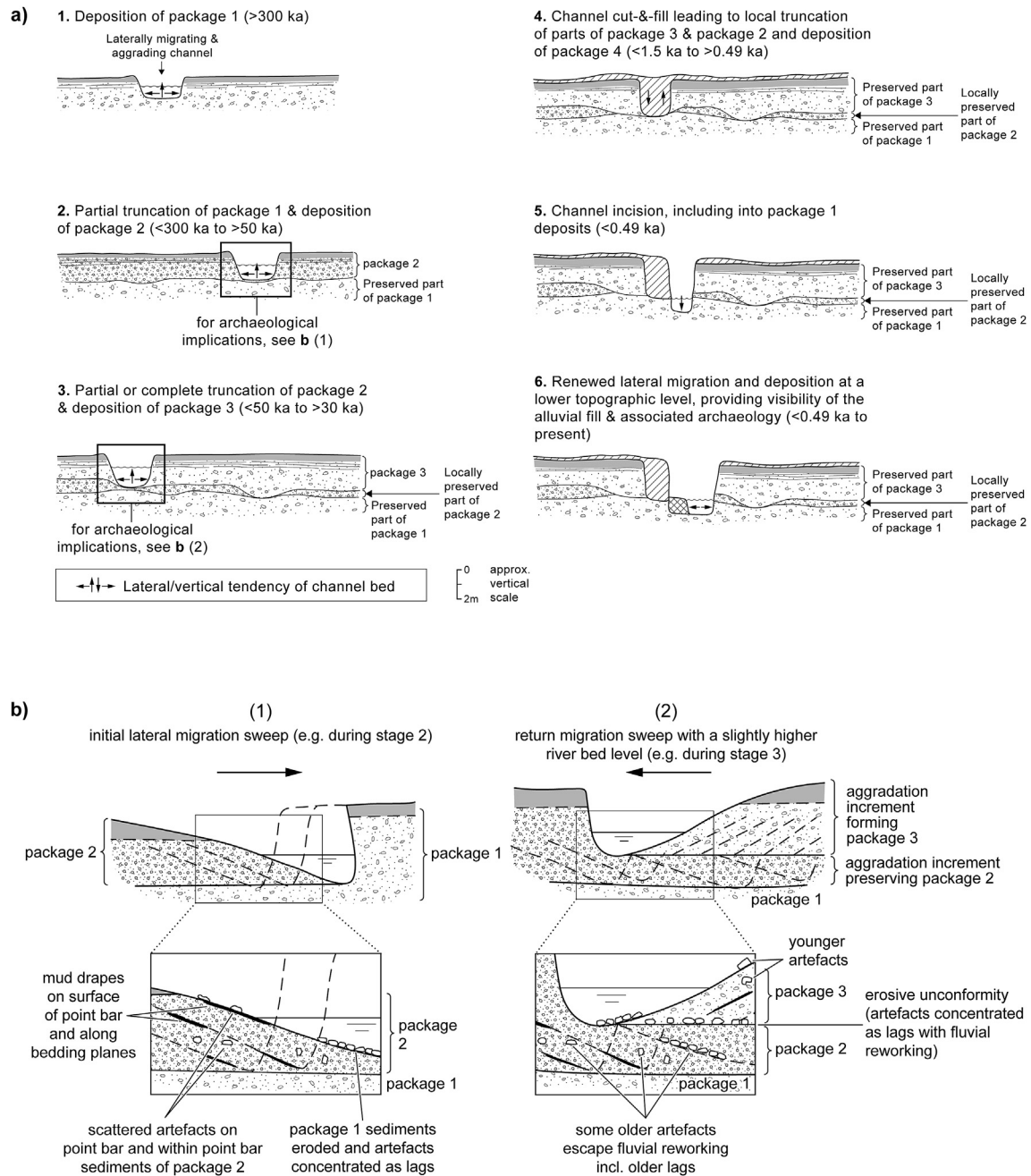
Figure 15. a) Schematic diagram illustrating a conceptual model for the development of the fluvial succession found at Site C North in the central Kalambo Basin. Six stages of river activity have led to the deposition and exposure of four main sedimentary packages, with packages 1–3 being especially rich in archaeological terms. b) Schematic diagram showing the implications of this model for the generation and preservation of the archaeological record (adapted from Lewin and Macklin (2003) and Barham et al. 2015). The record is characterised by scattered artefacts and lags that nonetheless retain chronological coherence in vertical succession.

5.2. Implications of fluvial activity for the archaeological record

The proposed model for fluvial activity (Fig. 15a) has implications for interpretations of the generation, preservation, and visibility of the associated archaeological record in the centre of the Kalambo Basin. For example, repeated lateral migration and partial or complete truncation of older deposits means that potential for reworking of artefacts has been high, with few if any preserved in primary contexts, as was recognised in earlier work at the site (e.g., Schick, 2001). Nonetheless, because most sedimentary packages have been subject to only partial truncation during later river activity and many artefacts may not be transported far and instead

have been preserved as lags (e.g., at the channel base or on point bars), the archaeological record thus still retains a stratigraphic coherence, with older artefacts being found in lower layers and younger artefacts in upper layers (Fig. 15b). In such situations, the age of the sedimentary package in which artefacts are found provides a minimum age for those artefacts, and the age of the underlying erosively truncated sedimentary package provides a maximum age for those artefacts.

Recent incision (Stage 5; Fig. 15a) and subsequent lateral migration (Stage 6) has been vital for the visibility of the archaeological record, for without these processes many artefacts would remain deeply buried and largely undetectable. Meander migration

and bank erosion provide both threats and opportunities; as we discovered during our investigations in the basin, such processes may consume older excavations (e.g., Clark's original Site C) but have also provided new exposures. If lateral migration continues into the near future, these natural processes may fortuitously expose other archaeological horizons that can be targeted with new excavations.

5.3. Significance of the Kalambo Falls archaeological record

The details of the archaeological record at Site C North are described elsewhere (Barham et al., 2015), with the key finding being a Mode 2/3 transition preserved in sedimentary package 1 that has been dated to ~500–300 ka. The mode concept, as modified by Shea (2011), is used in this study to highlight basic technological differences between archaeological horizons. This approach recognises that the sample sizes from Site C North are too small to make reliable attributions to the Stone Age industries defined for Kalambo Falls (Clark, 1969, 2001). At Site C North, Mode 2 (Acheulean) is recognised by the occurrence of large cutting tools (>10 cm) that include bifacially shaped handaxes and cleavers. Mode 3 (Middle Stone Age) is recognised by the occurrence of prepared cores and less direct indicators including platform preparation (Barham et al., 2015). Mode 2 artefacts occur only in sedimentary package 1, whereas Mode 3 artefacts occur in sedimentary packages 1, 2, and 3, with a re-deposited mixture of Stone Age and Iron Age artefacts found in the late Holocene channel deposits that define the major part of package 4.

Until now, reliable radiometric ages have been lacking for the late Acheulean and the earliest Middle Stone Age at Kalambo Falls. The TT-OSL results from Site C North place the transition well within the Middle Pleistocene, and the site can now be added to the small number of other dated Mode 2/3 transitions in southern and eastern Africa (Beaumont and Vogel, 2006; Tryon et al., 2006; Porat et al., 2010) and in southwest Asia (Gopher et al., 2010). Together, they provide evidence for increasing technological variability between ~500 and 300 ka that is characterised by the development of new forms of cores, blanks, and the invention of combinatorial tools (Johnston and McBrearty, 2010; Wilkins et al., 2012; Barham, 2013). Regional variability is also emerging in the duration of the Mode 2/3 transition (McBrearty and Tryon, 2006). In Ethiopia, cleavers and handaxes were still being made ~212 ka (de la Torre et al., 2014), whereas the TT-OSL chronology for Site C North suggests a potentially earlier cessation of these technologies in this part of south-central Africa.

Nascent regional differences such as this are only now becoming evident as a result of the development of radiometric dating methods. TT-OSL is of particular importance as it will enable archaeologists to generate chronological frameworks in areas where the options for the use of other dating techniques are limited by geological factors and by poor organic preservation. These limitations apply in particular to many of the Stone Age sites in central and west Africa (Barham and Mitchell, 2008). The archaeological succession at Kalambo Falls is important in this context, as it straddles the gap between the better dated sites in eastern and southern Africa, and offers large existing collections of Mode 2 and Mode 3 artefacts from deposits that can now be dated more reliably.

6. Conclusions

Although fluvial deposits such as terrace flights and basin and valley fills can provide key records of early hominin activity, interpretations are commonly hampered by uncertainties in fluvial process interpretations and by the difficulties in obtaining chronologies, especially for older sites beyond the range of radiocarbon. Prior to this study, an appreciation of the significance of the Kalambo Falls archaeological site had been restricted, particularly by the lack of a reliable chronology, thereby contributing to the site's marginalisation in discussions about the timing and importance of the technological transition from the Acheulean to the Middle Stone Age (e.g., McBrearty, 2001). Using a combination of OSL and TT-OSL, we have provided a chronology for the fluvial succession in the central part of the Kalambo Basin. This chronology reveals a punctuated depositional record, characterised by four temporally distinct sedimentary packages (age ranges of ~500–300 ka, ~300–50 ka, ~50–30 ka, and ~1.5–0.49 ka). Combining this chronology with insights derived from geomorphology and sedimentology has enabled development of a conceptual model that can be used to interpret the generation, preservation, and visibility of the archaeological record at Site C North. Importantly, although deposition has been punctuated and the assemblage of sedimentary packages is complex, the associated archaeological record has retained stratigraphic coherence.

These findings provide a springboard from which to initiate further archaeological investigations in the area and will help Kalambo Falls regain its place among the pre-eminent Stone Age sites in Africa. The combination of geomorphological, sedimentological, and geochronological approaches employed in this study also demonstrates the potential for investigations of other fluvial archaeological sites, both in Africa and farther afield. In particular, where suitable quartz-rich deposits are present, the combined use of OSL and TT-OSL signals offers the potential for establishing chronological control perhaps extending back over half a million years.

References

Adamiec, G., Duller, G.A.T., Roberts, H.M., Wintle, A.G., 2010. Improving the TT-OSL SAR protocol through source trap characterisation. Radiat. Measurements 45, 768–777.

Armitage, S.J., Jasim, S.A., Marks, A.E., Parker, A.G., Usik, V.I., Uerpmann, H.P., 2011. The southern route "Out of Africa": evidence for an early expansion of modern humans into Arabia. Science 331, 453–456.

Arnold, L.J., Demuro, M., Parés, J.M., Luis Arsuaga, J., Aranburu, A., Bermúdez de Castro, J.M., Carbonell, E., 2014. Luminescence dating and palaeomagnetic age constraint on hominins from Sima de los Huesos, Atapuerca. Spain. J. Hum. Evol. 67, 85–107.

Barham, L., 2013. From Hand to Handle: The First Industrial Revolution. Oxford University Press, Oxford.

Barham, L., Mitchell, P., 2008. The First Africans: African Archaeology from the Earliest Toolmakers to Most Recent Foragers. Cambridge University Press, Cambridge.

Barham, L., Duller, G.A.T., Plater, A.J., Tooth, S., Turner, S., 2009. Recent excavations at Kalambo Falls, Zambia. Antiquity 83 (322).

Barham, L., Tooth, S., Duller, G.A.T., Plater, A.J., Turner, S., 2015. Excavations at Site C North, Kalambo Falls, Zambia: new insights into the Mode 2/3 transition in south-central Africa. J. Afr. Archaeol. 13 (2) http://dx.doi.org/10.3213/2191-5784-10270.

Beaumont, P.B., Vogel, J.C., 2006. On a timescale for the past million years of human history in central South Africa. S. Afr. J. Sci. 102, 217–228.

Bond, G., 1969. Appendix A. The Geology of the Kalambo Falls Prehistoric Site. In: Clark, J.D. (Ed.), Kalambo Falls Prehistoric Site, Volume I. Cambridge University Press, Cambridge, pp. 197–214.

Bøtter-Jensen, L., Andersen, C.E., Duller, G.A.T., Murray, A.S., 2003. Developments in radiation, stimulation and observation facilities in luminescence measurements. Radiation Measurements 37, 535–541.

Bridgland, D.R., 2006. The Middle and Upper Pleistocene sequence in the Lower Thames: a record of Milankovitch climatic fluctuation and early human occupation of southern Britain - Henry Stopes Memorial Lecture 2004. Proc. Geol. Assoc. 117, 281–305.

Brink, J.S., Herries, A.I.R., Moggi-Cecchi, J., Gowlett, J.A.J., Bousman, C.B., Hancox, J.P., Grün, R., Eisenmann, V., Adams, J.W., Rossouw, L., 2012. First hominine remains from a ~ 1.0 million year old bone bed at Cornelia-Uitzoek, Free State Province, South Africa. J. Hum. Evol. 63, 527–535.

Chapot, M.S., Roberts, H.M., Duller, G.A.T., Lai, Z.P., 2012. A comparison of natural- and laboratory-generated dose response curves for quartz optically stimulated luminescence signals from Chinese loess. Radiation Measurements 47, 1045–1052.

Clark, J.D., 1969. Kalambo Falls Prehistoric Site, Volume I. Cambridge University Press, Cambridge.

Clark, J.D., 2001. Kalambo Falls Prehistoric Site, Volume III. Cambridge University Press, Cambridge.

Clark-Balzan, L.A., Candy, I., Schwenninger, J.-L., Bouzouggar, A., Blockley, S., Nathan, R., Barton, R.N.E., 2012. Coupled U-series and OSL dating of a Late Pleistocene cave sediment sequence, Morocco, North Africa: significance for constructing Palaeolithic chronologies. Quatern. Geochronol 12, 53–64.

Duller, G.A.T., 2004. Luminescence dating of Quaternary sediments: recent advances. J. Quatern. Sci. 19, 183–192.

Duller, G.A.T., 2008a. Luminescence Dating: Guidelines on Using Luminescence Dating in Archaeology. English Heritage, Swindon.

Duller, G.A.T., 2008b. Single grain optical dating of Quaternary sediments: why aliquot size matters in luminescence dating. Boreas 37, 589–612.

Duller, G.A.T., 2012. Improving the accuracy and precision of equivalent doses determined using the optically stimulated luminescence signal from single grains of quartz. Radiation Measurements 47, 770–777.

Duller, G.A.T., Wintle, A.G., 2012. The potential of the thermally transferred optically stimulated luminescence signal from quartz for dating sediments. Quatern. Geochronol 7, 6–20.

Erlanger, E.D., Granger, D.E., Gibbon, R.J., 2012. Rock uplift rates in South Africa from isochron burial dating of fluvial and marine terraces. Geology 40, 1019–1022.

Galbraith, R.F., Roberts, R.G., Laslett, G.M., Yoshida, H., Olley, J.M., 1999. Optical dating of single and multiple grains of quartz from Jinmium rock shelter, northern Australia: Part I, Experimental design and statistical models. Archaeometry 41, 339–364.

Gibbon, R.J., Granger, D.E., Kuman, K., Partridge, T.C., 2009. Early Acheulean technology in the Rietputs Formation, South Africa, dated with cosmogenic nuclides. J. Hum. Evol. 56, 152–160.

Gopher, A., Ayalon, A., Bar-Matthews, M., Barkai, R., Frumkin, A., Karkanas, P, Shahack-Gross, R., 2010. The chronology of the Later Lower Palaeolithic in the Levant based on the U-Th ages of speleothem from Qesem Cave, Israel. Quatern. Geochronol 5, 644–656.

Haldemann, E.G., 1969. Chapter 2, Part I: Geological and physiographical setting of the Kalambo Falls prehistoric site. In: Clark, J.D. (Ed.), Kalambo Falls Prehistoric Site, Volume I. Cambridge University Press, Cambridge, pp. 20–46.

Hu, G., Zhang, J.-F., Qiu, W.-L., Zhou, L.P., 2010. Residual OSL signals in modern fluvial sediments from the Yellow River (HuangHe) and the implications for dating young sediments. Quatern. Geochronol 5, 187–193.

Jacobs, Z., Duller, G.A.T., Wintle, A.G., 2006. Interpretation of single grain D_e distributions and calculation of D_e. Radiation Measurements 41, 264–277.

Jacobs, Z., Roberts, R.G., 2007. Advances in optically stimulated luminescence (OSL) dating of individual grains of quartz from archaeological deposits. Evol. Anthropol 16, 210–223.

Jacobs, Z., Roberts, R.G., Galbraith, R.F., Deacon, H.J., Grün, R., Mackay, A.W., Mitchell, P., Vogelsang, R., Wadley, L., 2008. Ages for the Middle Stone Age of Southern Africa: Implications for human behavior and dispersal. Science 322, 733–735.

Jacobs, Z., Roberts, R.G., Lachlan, T.J., Karkanas, P., Marean, C.W., Roberts, D.L., 2011. Development of the SAR TT-OSL procedure for dating Middle Pleistocene dune and shallow marine deposits along the southern Cape coast of South Africa. Quatern. Geochronol. 6, 491–513.

Jain, M., Murray, A.S., Bøtter-Jensen, L., 2004. Optically stimulated luminescence dating: how significant is incomplete light exposure in fluvial environments? Quaternaire 15, 143–157.

Johnston, C.R., McBrearty, S., 2010. 500,000 year old blades from the Kapthurin Formation, Kenya. J. Hum. Evol. 58, 193–200.

Kim, J.C., Duller, G.A.T., Roberts, H.M., Wintle, A.G., Lee, Y.I., Yi, S.B., 2010. Re-evaluation of the chronology of the palaeolithic site at Jeongokri, Korea, using OSL and TT-OSL signals from quartz. Quatern. Geochronol. 5, 365–370.

Lee, C., Bada, J.L., Peterson, E., 1976. Amino-acids in modern and fossil woods. Nature 259, 183–186.

Lewin, J., Macklin, M.G., 2003. Preservation potential for Late Quaternary river alluvium. J. Quatern. Sci. 18, 107–120.

Lyons, R.G., Tooth, S., Duller, G.A.T., 2014. Late Quaternary climatic changes revealed by luminescence dating, mineral magnetism and diffuse reflectance spectroscopy of river terrace palaeosols: a new form of geoproxy data for the southern African interior. Quatern. Sci. Rev. 95, 43–59.

Macklin, M.G., Tooth, S., Brewer, P.A., Noble, P.L., Duller, G.A.T., 2010. Holocene flooding and river development in a Mediterranean steepland catchment: the Anapodaris Gorge, south-central Crete, Greece. Global Planet. Change 70, 35–52.

McBrearty, S., 2001. The Middle Pleistocene of east Africa. In: Barham, L.S., Robson-Brown, K. (Eds.), Human roots: Africa and Asia in the Middle Pleistocene. Western Academic and Specialist Press, Bristol, pp. 81–98.

McBrearty, S., Tryon, C., 2006. From Acheulean to Middle Stone Age in the Kapthurin Formation, Kenya. In: Hovers, E., Kuhn, S. (Eds.), Transitions Before the Transition: Evolution and Stability in the Middle Paleolithic and Middle Stone Age. Springer, New York, pp. 257–277.

McKinney, C., 2001. Appendix D: The uranium-series age of wood from Kalambo Falls. In: Clark, J.D. (Ed.), Kalambo Falls Prehistoric Site, Volume III. Cambridge University Press, Cambridge.

Mercier, N., Falguères, C., 2007. Field gamma dose-rate measurement with a NaI(Tl) detector: re-evaluation of the "threshold" technique. Ancient TL 25, 1–4.

Mishra, S., White, M.J., Beaumont, P., Antoine, P., Bridgland, D.R., Limondin-Lozouet, N., Santisteban, J.I., Schreve, D.C., Shaw, A.D., Wenban-Smith, F.F., Westaway, R.W.C., White, T.S., 2007. Fluvial deposits as an archive of early human activity. Quatern. Sci. Rev. 26, 2996–3016.

Murray, A.S., Olley, J.M., 2002. Precision and accuracy in the optically stimulated luminescence dating of sedimentary quartz: a status review. Geochronometria 21, 1–16.

Penkman, K.E.H., Preece, R.C., Bridgland, D.R., Keen, D.H., Meijer, T., Parfitt, S.A., White, T.S., Collins, M.J., 2011. A chronological framework for the British Quaternary based on Bithynia opercula. Nature 476, 446–449.

Petraglia, M., Korisettar, R., Boivin, N., Clarkson, C., Ditchfield, P., Jones, S., Koshy, J., Lahr, M.M., Oppenheimer, C., Pyle, D., Roberts, R., Schwenninger, J.L., Arnold, L., White, K., 2007. Middle Paleolithic assemblages from the Indian subcontinent before and after the Toba super-eruption. Science 317, 114–116.

Porat, N., Chazan, M., Grün, R., Aubert, M., Eisenmann, V., Horwitz, L.K., 2010. New radiometric ages for the Fauresmith industry from Kathu Pan, southern Africa: implications for the Earlier to Middle Stone Age transition. J. Archaeol. Sci. 37, 269–283.

Prescott, J.R., Hutton, J.T., 1994. Cosmic ray contributions to dose rates for luminescence and ESR dating: large depths and long-term time variations. Radiation Measurements 23, 497–500.

Rhodes, E.J., 2011. Optically stimulated luminescence dating of sediments over the past 200,000 years. Ann. Rev. Earth Planet. Sci. 39, 461–488.

Rittenour, T.M., 2008. Luminescence dating of fluvial deposits: applications to geomorphic, palaeoseismic and archaeologic work. Boreas 37, 613–635.

Rodnight, H., Duller, G.A.T., Tooth, S., Wintle, A.G., 2005. Optical dating of a scroll-bar sequence on the Klip River, South Africa, to derive the lateral migration rate of a meander bend. The Holocene 15, 802–811.

Rosina, P., Voinchet, P., Bahain, J.J., Cristovao, J., Falgueres, C., 2014. Dating the onset of Lower Tagus River terrace formation using electron spin resonance. J. Quatern. Sci. 29, 153–162.

Schick, K.D., 2001. An examination of Kalambo Falls Acheulean Site B5 from a geoarchaeological perspective. In: Clark, J.D. (Ed.), Kalambo Falls Prehistoric Site, volume III. Cambridge University Press, Cambridge, pp. 463–480.

Schreve, D.C., Bridgland, D.R., Allen, P., Blackford, J.J., Gleed-Owen, C.P., Griffiths, H.I., Keen, D.H., White, M.J., 2002. Sedimentology, palaeontology and archaeology of late Middle Pleistocene River Thames terrace deposits at Purfleet, Essex, UK. Quatern. Sci. Rev. 21, 1423–1464.

Shea, J.J., 2011. Homo sapiens is as Homo sapiens was: behavioural variability versus "behavioral modernity" in Paleolithic archaeology. Curr. Anthropol 52, 1–35.

Sheppard, P.J., Kleindienst, M.R., 1996. Technological change in the Earlier and Middle Stone Age of Kalambo Falls (Zambia). Afr. Archaeol. Rev. 13, 171–196.

Taylor, R.E., 1987. Radiocarbon dating: an archaeological perspective. Academic Press, London.

Thiel, C., Buylaert, J.-P., Murray, A.S., Elmejdoub, N., Jedoui, Y., 2012. A comparison of TT-OSL and post-IR IRSL dating of coastal deposits on Cap Bon peninsula, north-eastern Tunisia. Quatern. Geochronol 10, 209–217.

Tierney, J.E., Russell, J.M., Huang, Y., Damste, J.S.S., Hopmans, E.C., Cohen, A.S., 2008. Northern hemisphere controls on tropical southeast African climate during the past 60,000 years. Science 322, 252–255.

Tooth, S., Hancox, P.J., Brandt, D., McCarthy, T.S., Jacobs, Z., Woodborne, S., 2013. Controls on the genesis, sedimentary architecture, and preservation potential of dryland alluvial successions in stable continental interiors: insights from the incising Modder River, South Africa. J. Sediment. Res. 83, 541–561.

de la Torre, I., Mora, R., Arroyo, A., Benito-Calvo, A., 2014. Acheulean technological behaviour in the Middle Pleistocene landscape of Mieso (East-Central Ethiopia). J. Hum. Evol. 76, 1–25.

Tryon, C.A., McBrearty, S., Texier, J.-P., 2006. Levallois lithic technology from the Kapthurin Formation, Kenya: Acheulian origin and Middle Stone Age diversity. Afr. Archaeol. Rev. 22, 199–229.

Tsukamoto, S., Duller, G.A.T., Wintle, A.G., 2008. Characteristics of thermally transferred optically stimulated luminescence (TT-OSL) in quartz and its potential for dating sediments. Radiation Measurements 43, 1204–1218.

Wilkins, J., Schoville, B.J., Brown, K.S., Chazan, M., 2012. Evidence for early hafted hunting technology. Science 388, 942–946.

Wintle, A.G., Murray, A.S., 2006. A review of quartz optically stimulated luminescence characteristics and their relevance in single-aliquot regeneration dating protocols. Radiation Measurements 41, 369–391.

Woltering, M., Johnson, T.C., Werne, J.P., Schouten, S., Damste, J.S.S., 2011. Late Pleistocene temperature history of Southeast Africa: A TEX_{86} temperature record from Lake Malawi. Palaeogeogr. Palaeoclimatol. Palaeoecol 303, 93–102.